Science of Sintering, **56** (2024) 269-283

https://doi.org/10.2298/SOS231003060O

UDK: 622.785; 692.533.1; 539.375

Influence of Different Sintering Techniques on the Wear Properties of Al-15Si-2.5Cu-0.5Mg/B_4C Composites

Melika Ozer[1], Yavuz Kaplan[2], Alpay Ozer[1], Sinan Aksoz[3*)]

[1]Metallurgical and Materials Engineering, Faculty of Technology, Gazi University, 06560, Ankara, Türkiye

[2]Manufacturing Engineering, Faculty of Technology, Pamukkale University, 06560, Denizli, Türkiye

[3]Metallurgical and Materials Engineering, Faculty of Technology, Pamukkale University, 06560, Denizli, Türkiye

Abstract:

In this study, the influences of different sintering techniques and B_4C particle addition on microstructural properties, density, hardness and abrasive wear were investigated. The wear experiments were carried out in accordance with ASTM standard G99 using a pin-on-disk apparatus under dry test conditions. Compact samples produced with conventional and microwave sintering gave density and hardness values close to each other. In compacts produced with the spark plasma sintering technique, the porosity rate is the lowest, and the hardness is the highest. In samples produced with different sintering techniques, the addition of B_4C particles caused an increase in porosity and decreased density and hardness. The lowest wear resistance in all samples was determined in samples produced by conventional sintering. The lowest volume loss, that is, the highest wear resistance, was obtained in the samples produced with spark plasma sintering. In general, adding B_4C negatively affected the wear performance in all samples.

Keywords*: Sintering; Wear; Composite; Al alloy.*

1. Introduction

Composite materials, which are widely used especially in the aerospace, military, and automobile industries and are classified as advanced engineering materials, have become a necessity for modern production technology [1-4]. The most important advantage of composite materials is that they are lightweight and have high mechanical properties [5-7]. Especially their high specific strength makes composite materials attractive engineering materials [7-9]. Composite materials can have these properties by choosing the appropriate matrix material and reinforcement element. Using aluminum alloys as matrix materials, composites with high specific strength can be produced. While the use of hypereutectic Al-Si alloys has increased in recent years as matrix materials due to their properties, such as high wear resistance and strength, the number of research on these Al alloys has also increased [10-13].

Composite materials are produced using different powder metallurgy (P/M) techniques. Cold pressing and sintering are one of the most common P/M techniques known

*) **Corresponding author:** sinanaksoz1984@gmail.com

[14,15]. However, sintering techniques that save energy and time have gained importance in recent years. New sintering technologies promise rapid heating, low energy costs, and new microstructures. New sintering techniques include microwave, plasma, and induction sources. Sintering techniques have effects on the characteristics and mechanical properties of P/M compacts. By improving mechanical properties, wear resistance can be increased [8,16, 17].
In this study, the influences of different sintering techniques and B_4C particle addition on microstructural properties, density, hardness, and wear performance were investigated. Due to their remarkable properties, hypereutectic Al-Si alloy powders were chosen as matrix material and boron carbide particles in B_4C composition were used as reinforcement. Hypereutectic Al/Si alloy compacts, and Al-Si/B_4C composites were produced using cold pressing+conventional sintering and cold pressing+microwave sintering and spark plasma sintering techniques. The advantages of spark plasma sintering (SPS) and microwave sintering (MWS), which are fast sintering techniques compared to conventional sintering (CS) are discussed.

2. Materials and Experimental Procedures

2.1. Material

Al-Si compacts and B_4C-reinforced hypereutectic Al-Si matrix composites were produced by CS, MWS, and SPS techniques. Hypereutectic Al-Si (ECKA Granulate Velden GmbH) powders, whose trade name is Alumix 231®, were used as the metal matrix material. The average size of Alumix 231® alloy powders produced by the gas atomization method is D_{50} ~75µm, D_{10} ~22 µm and D_{90} ~190 µm. B_4C particles with an average grain size of 10 µm (D_{50}) were used as reinforcement elements in the matrix material. The chemical composition and recommended pressing-sintering conditions of Alumix 231®, whose sintered density is 2.67 g/cm^3, are given in Table I.

Tab. I Chemical composition of Alumix 231® (wt.%) and pressing-sintering conditions.

Alumix 231®		Al	Si	Cu	Mg	Lubr. Amidwax
	Nominal target	Balance	14-16	2.4-2.8	0.5-0.8	1.5
	Experimental	Balance	15.4	3.05	0.57	
Compacting:	Compacting Pressure		620 MPa		Green density: 2.48 g/cm^3	
Sintering:	Dewaxing		380-420 °C			
	Sintering temperature		550-560 °C		Sintered density: 2.67 g/cm^3	
	Sintering time		approx. 60 min			
	Atmosphere		N_2			

2.2. Method

2.2.1. Mixing and pressing of powders

For the production of particle-reinforced composite material, a B_4C reinforcement element was added to the matrix material at a rate of 10% by weight. The prepared powder mixtures were blended in a triaxial mixer for 45 min. Powders prepared for CS and MWS processes were cold pressed by applying 620 MPa pressure with a unidirectional hydraulic press at room temperature. The lubricant removal process was applied to the pressed samples and those prepared for SPS. This process was completed by holding time for 20 min at 400 °C.

2.2.2. Sintering processes

CS process was carried out in N_2 atmosphere at a heating rate of 5 °C.min^{-1} and a temperature of 555 °C, using a Protherm brand tube furnace. The holding time at the sintering temperature was 60 min, and the samples were cooled in air. MWS process was carried out in a Synotherm brand atmosphere-protected laboratory-type microwave oven with a heating rate of 10 °C.min^{-1}. The samples were sintered at a sintering temperature of 555 °C and without holding time at this temperature. For SPS, 25 g of powder was charged into the mold, and a preload of 1 MPa was applied. The powders were sintered at 450 °C for 5 min by applying 50 MPa pressing pressure. Sintering was carried out in a vacuum environment at a heating rate of 100 °C.min^{-1}. Table II illustrates the specimen notations of the samples.

Tab. II The specimen notations of the samples.

Specimen	Materials	Sintering	Sintering temperature (°C)	Sintering time (min)
CS-555/60	Alumix 231®	Conventional	555	60
10-CS-555/60	Alumix 231® +10wt.%B_4C	Conventional	555	60
MWS-555/0	Alumix 231®	Microwave	555	0
10-MWS-555/0	Alumix 231® +10wt.%B_4C	Microwave	555	0
SPS-450/5	Alumix 231®	Spark Plasma	450	5
10-SPS-450/5	Alumix 231® +10wt.%B_4C	Spark Plasma	450	5

2.2.3. Microstructural analysis

For microstructural analysis, the samples were subjected to standard metallographic grinding processes. Keller's etcher was used for etching the samples. The microstructures of the prepared samples were imaged and analyzed by optical microscope and scanning electron microscope (SEM).

2.2.4. Density measurement

The densities of green and sintered samples obtained by pressing and sintering processes were measured with the Archimedes' technique according to ASTM B962-08 standard. Densities are reported as relative density (rd%) in proportion to the theoretical density value. Theoretical density was calculated according to the mixture rule using the material composition.

2.2.5. Hardness measurements and pin-on-disc wear experiments

Macro hardness tests of the samples were performed using the Brinell hardness method (Emcotest Duravision). Hardness measurements were performed with a load of 31.5 kgf and a hardened steel indenter ball with a diameter of 2.5 mm. Ten measurements were carried out on each sample. The arithmetic averages of the measurement results were used.

The wear experiments were performed in accordance with ASTM standard G99 using a pin-on-disk apparatus under dry test conditions. Al samples in Ø10x25 mm diameter were used as a pin and 60 HRC hardness 52100 steel as counter-face during the wear experiments. The wear experiments were carried out at 1 h sliding time under three different loads of 5, 10, and 15 N at a speed of 1 m.s^{-1}. The applied load on the specimen was recorded during the wear test to calculate the friction coefficient. The friction coefficient was calculated using Equation (1).

The coefficient of friction is $\mu = \frac{F}{P}$ (1)

F and P, respectively, symbolize the frictional force and the normal load on the specimen. Equation (2) explains how to calculate volume loss from the weight loss.

$$Volume\ Loss\ (mm^3) = \frac{Weight\ Loss\ (g)}{Density\ (g/mm^3)} \quad (2)$$

Equation (3) was used to define the specific wear rate.

$$Specific\ Wear\ rate\ (mm^3/Nm) = \frac{Volume\ Loss\ (mm^3)}{Sliding\ Distance\ (m)\ x\ Load\ (N)} \quad (3)$$

After the wear experiments, the worn surfaces were analyzed using field emission scanning electron microscopy (FESEM) and element dispersion spectroscopy (EDS), and surface damages were examined. Analyzes were carried out with a Zeiss brand and Supra 40VP model FESEM device.

3. Results and Discussion

3.1. Material and Microstructure Characterization

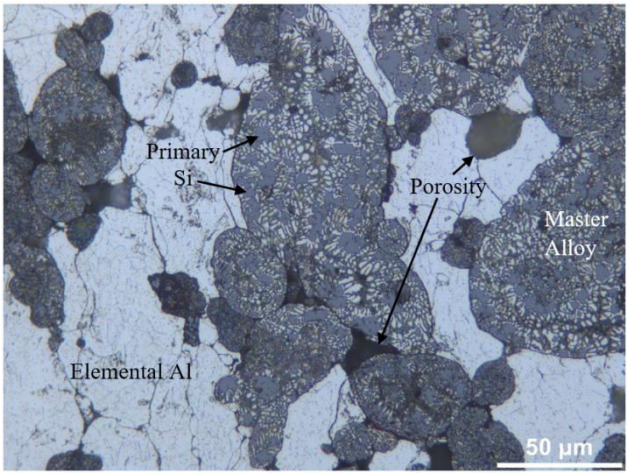

Fig. 1. Optical microscope micrograph of green Alumix 231®.

Powder mixtures prepared for producing Al-Si compacts and B_4C-reinforced hypereutectic Al-Si matrix composites were unidirectionally cold pressed by applying a pressure of 620 MPa. Cold-pressed samples were sintered with CS and MWS techniques. Additionally, Al-Si powders and Al-Si/B_4C mixture powders were sintered using the spark plasma technique, and compact samples were produced. Fig. 1 shows the optical microscope micrograph of green Alumix 231®. The microstructure consists of two light and dark-colored regions. The light-colored region is grains formed by elemental Al powders containing low amounts of Si, Cu, and Mg. The dark-colored areas are the original master alloy consisting of the Al-Si-Cu-Mg component. Therefore, Alumix 231® is a pre-alloyed mixture of P/M powder consisting of a mixture of elemental aluminum and original master alloy (Al-Si-Cu-Mg) powders. In the dark areas formed by the original master alloy powders, there are grayish large particles and finely distributed white particles of different sizes. It has been stated in the literature that grayish coarse particles are primary-Si particles grown from the master alloy

powder [4,12,18]. In addition, fine, white shiny particles are secondary phases rich in Cu. It can be said that these Cu-rich secondary phases are distributed in the form of precipitates. It has been stated in the literature that structures rich in Cu content have θ ($CuAl_2$) and γ (Al_2CuMg) secondary phases and that the Mg element exists as the β (Mg_2Si) secondary phase in the microstructure [9,18-22].

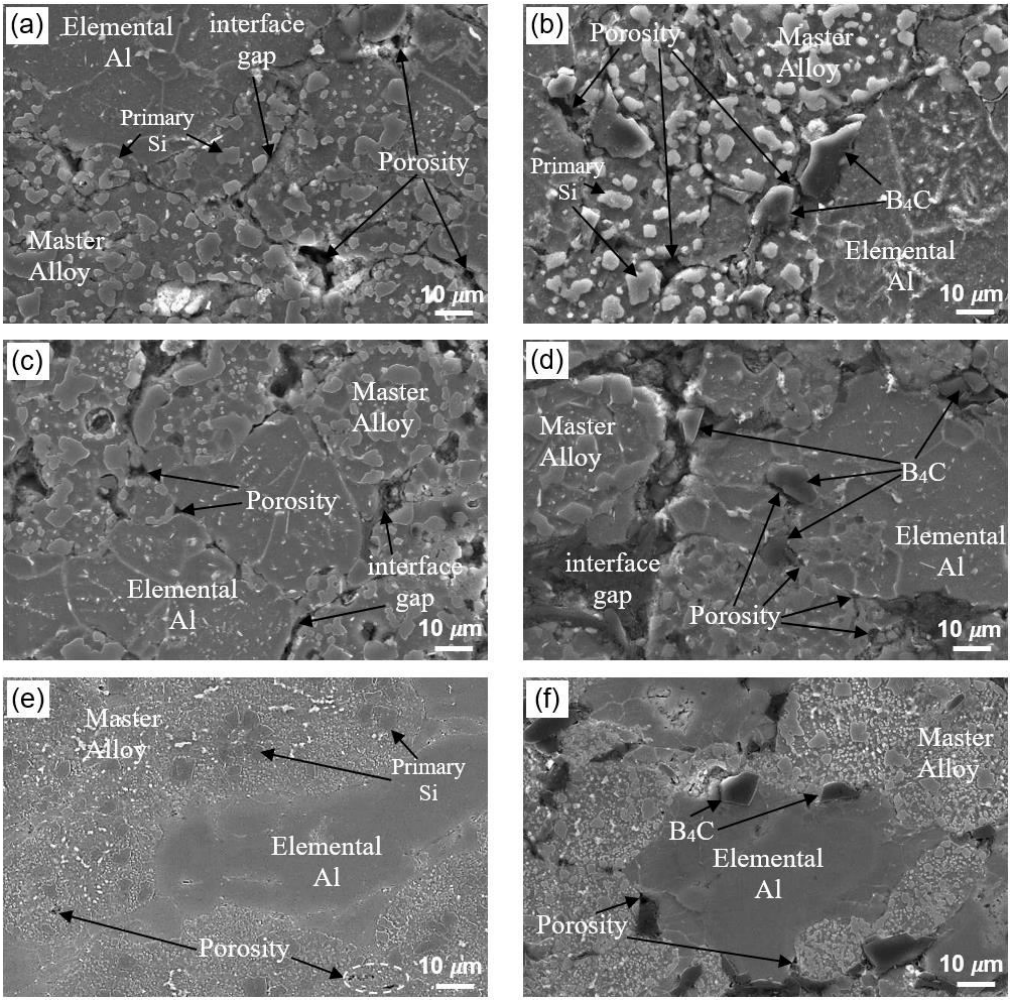

Fig. 2. SEM micrographs of samples (a) CS-555/60, (b) 10-CS-55/60, (c) MWS-555/0, (d) 10-MWS-555/0, (e) SPS-450/5, (f) 10-SPS-450/5.

SEM micrographs of the samples are given in Fig. 2. It was determined from the micrographs that similar structures (elemental Al, master alloy, primary Si) were formed in all samples depending on the matrix material. From the micrographs, it was determined that the porosity rate was highest in the sample produced with the MWS technique. However, considering the total volume of each sample, CS and MWS samples gave porosity values close to each other. The porosity rates of CS-555/60 and 10-CS-555/60 samples were calculated as 9.52% and 11.29%, respectively. The porosity rates of MWS-555/0 and 10-MWS-555/0 samples were calculated as 10.8% and 11.92%, respectively.

The samples with the lowest porosity rate is produced with SPS (Fig. 2e and f). SPS is a pressure sintering technique. In this study, the SPS process was carried out at 450 °C, 50 MPa pressure, and 5 min sintering time was carried out. In SPS, sparks formed at the contact points or gaps between the powders charged to the mold cause instantaneous regional

high temperatures and, therefore, evaporation and melting on the surfaces of the powder grains. The pressure applied during sintering eliminates and/or minimizes microspaces between powder grains and/or B_4C clusters [23-25]. When the micrographs of SPS-450/5 and 10-SPS-450/5 samples given in Figs 2e and f are examined, it is seen that the amount of porosity is relatively low and the existing pore size is smaller than other sintering techniques (porosity ratio ≈0.93%).

In addition, the intergranular coalescence problem seen in CS and MWS techniques was not detected in samples produced with SPS. However, in the sample produced with SPS, the porosity rate increased with the addition of B_4C (Fig. 2f). The porosity rate in the 10-SPS-450/5 sample is ≈2.35%. It was determined from micrographs that B_4C particles were found between elemental Al and/or master alloy grains and/or in pores in the composite samples produced by adding boron carbide. It can be seen from the micrographs that the interfacial bond between the matrix grains and the reinforcing B_4C particles is not formed and/or is partially formed. The high surface stresses of the ceramic particles used as reinforcement can be explained as the reason for this negativity. Therefore, it can be said that porosity increased with the addition of B_4C in all samples. The increase in porosity with the addition of B_4C is attributed to the incompatibility between the matrix grains and B_4C particles and the lack of a continuous and effective interface [24]. It is seen that the porosity amount in the samples sintered with CS and MWS is close to each other. The without holding time at the sintering in MWS is the superiority of this sintering technique over the CS technique.

3.2. Density and hardness analysis

The densities of the sintered samples were measured with Archimedes' technique by the ASTM B962-08 standard. Densities are reported as relative density. The hardness values of the samples were measured in Brinell hardness type. The density and hardness values of the samples are given in Fig. 3. In samples produced with different sintering techniques, an increase in porosity and a decrease in density were determined with the addition of B_4C particles. However, with the addition of B_4C, this decrease in intensities was limited to ≈2%. This decrease in densities is attributed to the pores between the matrix powder grains and the B_4C and/or B_4C particles. If the micrographs in Fig. 2 are examined, micropores formed between B_4C particles and the matrix will be seen in the samples with B_4C particle addition. When the density values of samples produced with different sintering techniques are compared, it can be seen in Fig. 3 that the samples produced with SPS give the highest density values. Samples produced with CS and MWS techniques gave similar density values.

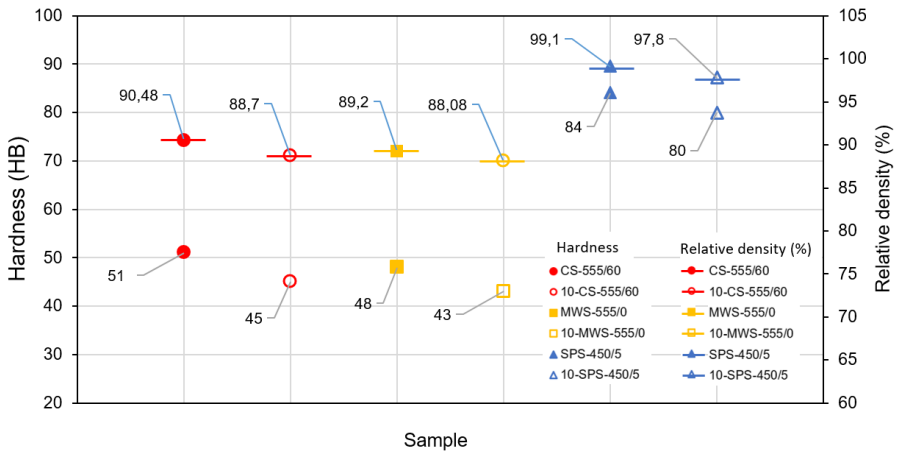

Fig. 3. Density and hardness changes in samples sintered with different techniques.

When the hardness data in Fig. 3 is examined, it is seen that CS and MWS samples give hardness values close to each other, consistent with the density data. CS-555/60 and MWS-555/0 gave hardness values of 51 HB and 48 HB, respectively. Samples 10-CS-555/60 and 10-MWS-55/0 also have hardness values of 45 HB and 43 HB, respectively. The values are close to each other regarding numerical data, and when CS and MWS samples are compared, the difference in hardness between them is ≈5%. Considering the effects of the hardness value of a metallic material on other mechanical properties, a difference of ≈5% in hardness values can have a significant impact value. However, it is an undeniable fact that MWS samples produced without holding time at the sintering temperature (0 min) offer a significant advantage in terms of saving time and energy. SPS samples, on the other hand, are the samples with the highest values in hardness data as well as density data due to the advantages of the production process. The addition of 10 wt% B_4C caused a decrease in hardness. Ozer et al. [24] stated that the increase in pore sizes and/or pore amount with the addition of B_4C caused this decrease in hardness.

3.3. Analysis of wear test results

The volume loss results of the Al-15Si-2,5 Cu-0.5Mg alloy sintered with different methods with and without B_4C reinforcement are given in Fig. 4. For both B_4C reinforced and unreinforced Al alloy, the highest volume loss and, thus, the lowest wear resistance were observed in the samples produced with CS. The lowest volume loss, i.e., the highest wear resistance, occurred in compact samples produced with SPS. The hardness values of unreinforced CS-555/60, MWS-555/0, SPS-450/5 samples are 51 HB, 48 HB and 84 HB, respectively. The hardness values of B_4C reinforced Al alloy are 45 HB, 43 HB and 80 HB, in the same order. Hardness is one of the most critical parameters affecting the tribological properties of the material [26-29]. However, wear test results also showed that hardness alone is not sufficient to increase wear resistance. Especially in P/M materials, the sintering process can affect all mechanical properties of the material [30-34]. Volume loss graphs also show that even if hardness values are close to each other, they can exhibit different wear behaviors. Although the hardness values of CS and MWS samples, both with and without B_4C reinforcement, were close to each other, the MWS method provided better wear resistance. In particular, B_4C reinforced MWS samples lost volume almost as much as SPS samples under 5 N and 10 N loads. This situation shows the importance of sintering in P/M materials.

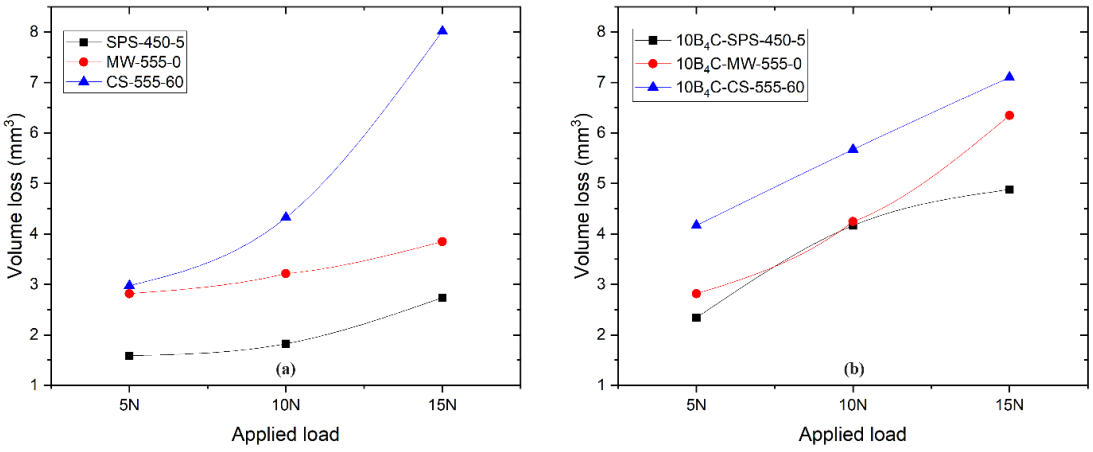

Fig. 4. Wear test volume loss results of samples (a) Unreinforced and b) B4C reinforced.

Specific wear rate (SWR) results of B_4C reinforced and unreinforced samples sintered with different methods are given in Fig. 5. SWR is an important tribological indicator that covers all wear parameters, such as applied load and sliding distance. SWR results are also similar to volume loss results. Among all wear test parameters, the highest wear rate was determined as approximately 23 mm^3/Nm in sample $10B_4C$-CS-555/60 under 5 N load. The lowest wear rate, approximately 5 mm^3/Nm, occurred in the SPS-450/5 sample under 10 N and 15 N loads. When the effect of 10 wt% B_4C reinforcement on the wear performance of Alumix 231® P/M compacts is examined, it is seen that the wear rates increase in three different sintering processes. According to the wear test results, the highest wear resistance was obtained by sintering with spark plasma. Then, the microwave sintering process and the worst wear resistance were obtained in conventional sintered samples.

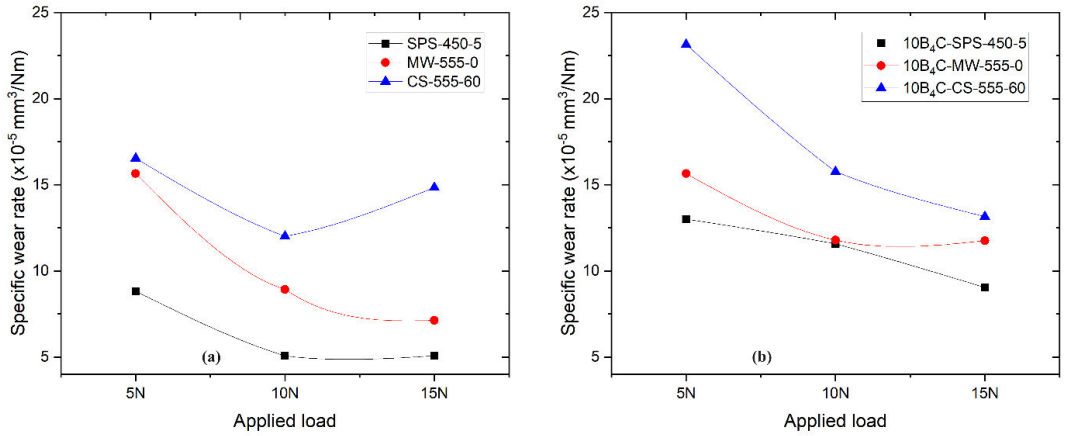

Fig. 5. SWR of Alumix 231® samples (a) Unreinforced and b) B_4C reinforced.

Fig. 6 shows the coefficient of friction (CoF) values recorded during the wear experiments. The numbers on the right side of the chart, in accordance with their colors, give the average CoF values for all test samples. Although there were some increases and decreases in CoF values, a generally smooth graph was obtained. B_4C reinforced, and unreinforced SPS Al alloy exhibited the lowest average CoF values. Al alloys produced with the SPS technique exhibited the most successful performance regarding volume loss and SWR values. No significant change was found in terms of CoF values among other sintering techniques.

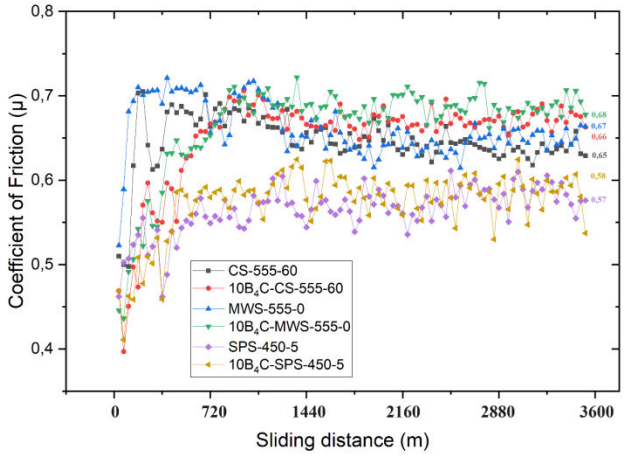

Fig. 6. CoF values during wear experiments.

If the general evaluation of the wear test results of the samples is made, the samples with the best wear performance are the samples produced with the SPS technique. Samples sintered with CS and MWS techniques were close to each other and exhibited lower wear performances than the SPS technique. These results are compatible with relative density and hardness values. The formation of a strong and gap-free interfacial bond between the matrix grains of SPS samples with high density and hardness values (Fig. 2e and b) enabled high wear performances to be obtained in these samples. The pores and bond deficiencies between the grains determined in the microstructures of the samples sintered with CS and MWS techniques (Fig. 2a-d) caused lower wear performances in these samples. The wear performances of CS, MWS and SPS samples were negatively affected by the addition of B_4C (except for the SPS-450-5 sample, which was subjected to the wear test with 15 N). It is explained in the 2.2 Material and Microstructure Characterization section that B_4C particles are located at the matrix grain boundaries and/or pores and that a strong interfacial bond is partially formed or/or not formed between the matrix grains and B_4C particles. It was stated that porosity increased with the addition of B_4C in all samples. In addition, the partial agglomeration of B_4C particles prevented these particles from forming a strong interfacial bond with the matrix. As a result of all these negativities, the addition of B_4C negatively affected the wear performance of the samples.

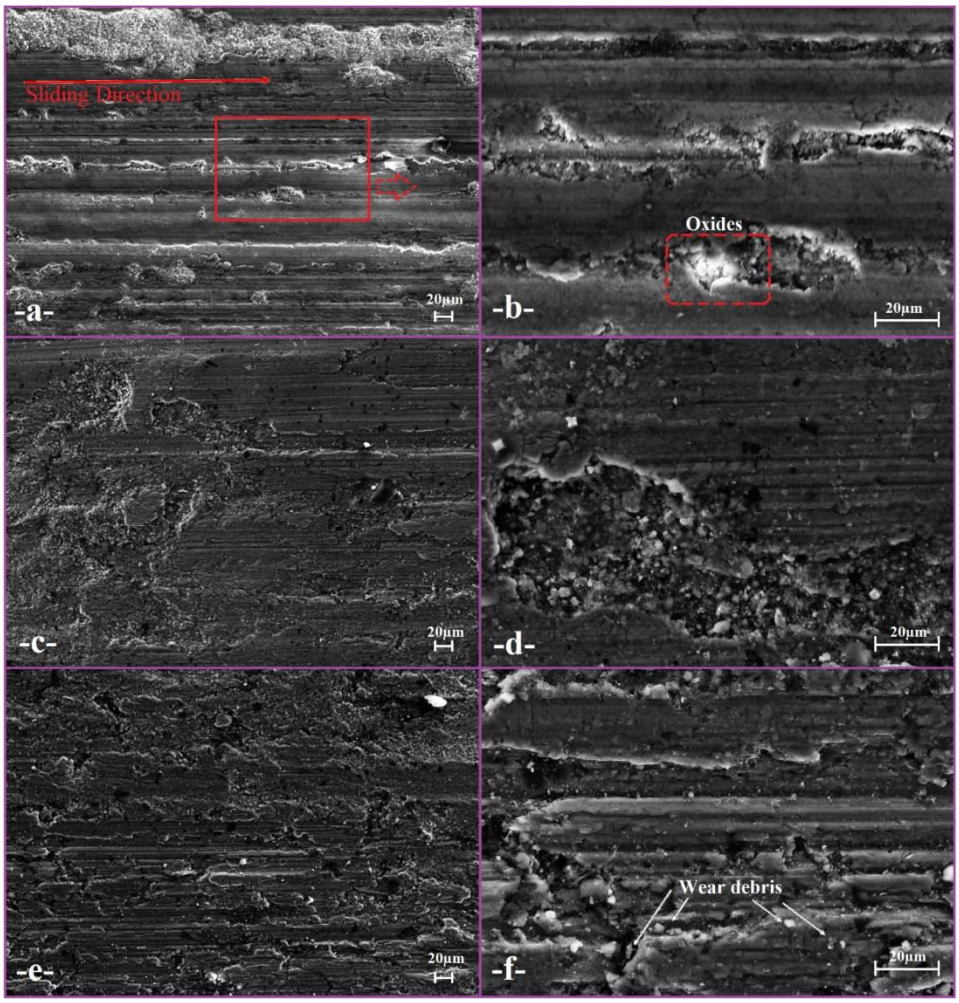

Fig. 7. FESEM images of the samples (a and b) CS-550/60, (c and d) 10-CS-55/60, (e and f) MWS-555/0.

In order to characterize the wear conditions and surface deformation effects, the worn surface FESEM images of the samples are given in Figs 7 and 8. When the worn surface FESEM images were examined, it was seen that there was post-wear oxidation in the structure. It is known that the oxide layer acts as a lubricant during wear and has a positive effect on wear behavior [35-38]. Depending on the sintering techniques, different worn surface images were formed on the samples after wear. It is observed that there are different wear errors, such as wear debris, adhesion, smearing, delimination, and ruptures after wear.

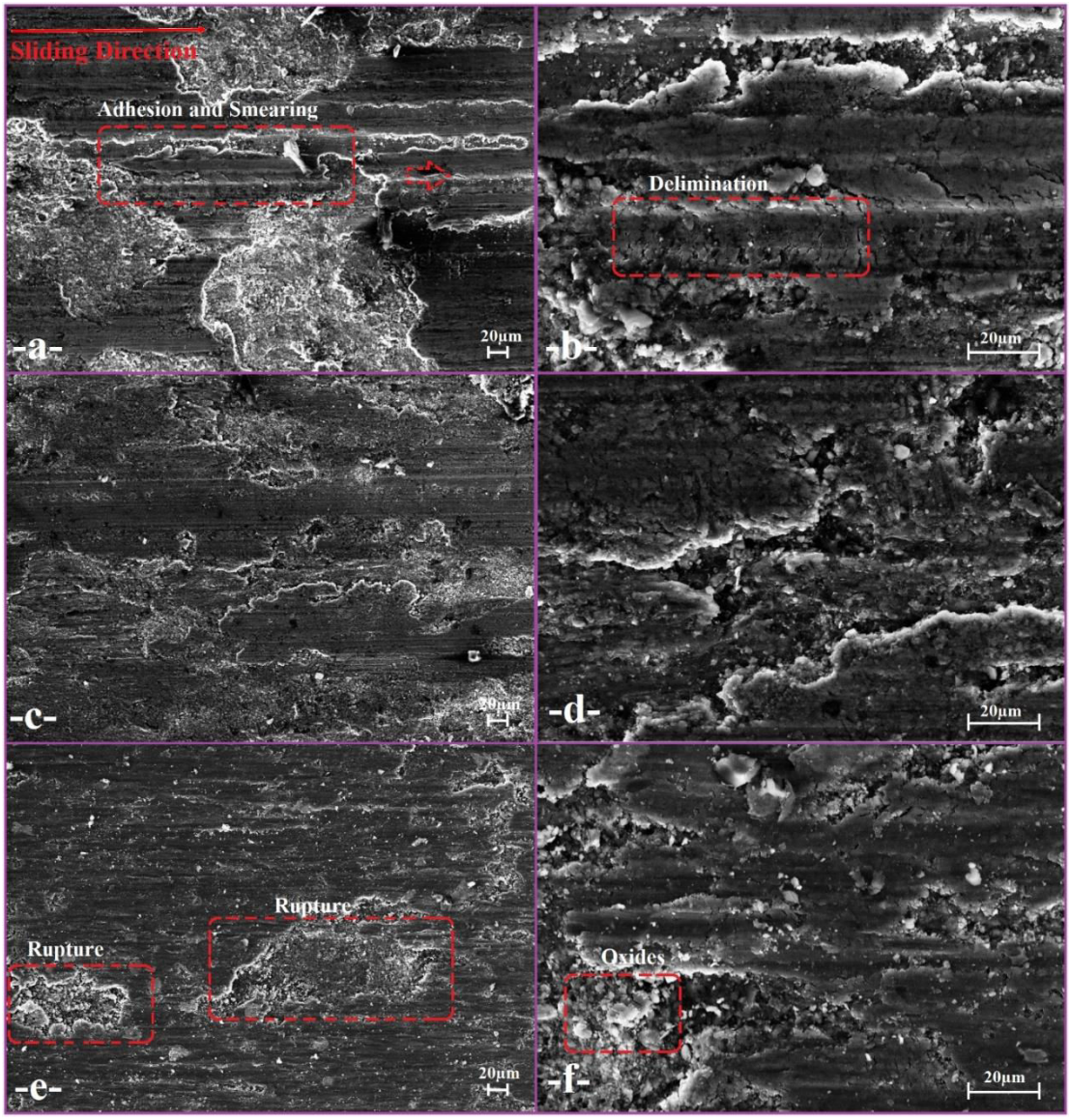

Fig. 8. FESEM images of the samples (a and b) 10-MWS-555/0, (c and d) SPS-450/5, (e and f) 10-SPS-450/5.

Fig. 9 shows the worn surface FESEM image of the samples and the element distribution graph taken from the FESEM image. In addition to the elements in the chemical composition of Alumix 231®, Fe and O elements were determined by EDS analysis. The O element showed its presence due to oxides formed on the exposed surface by corrosion.

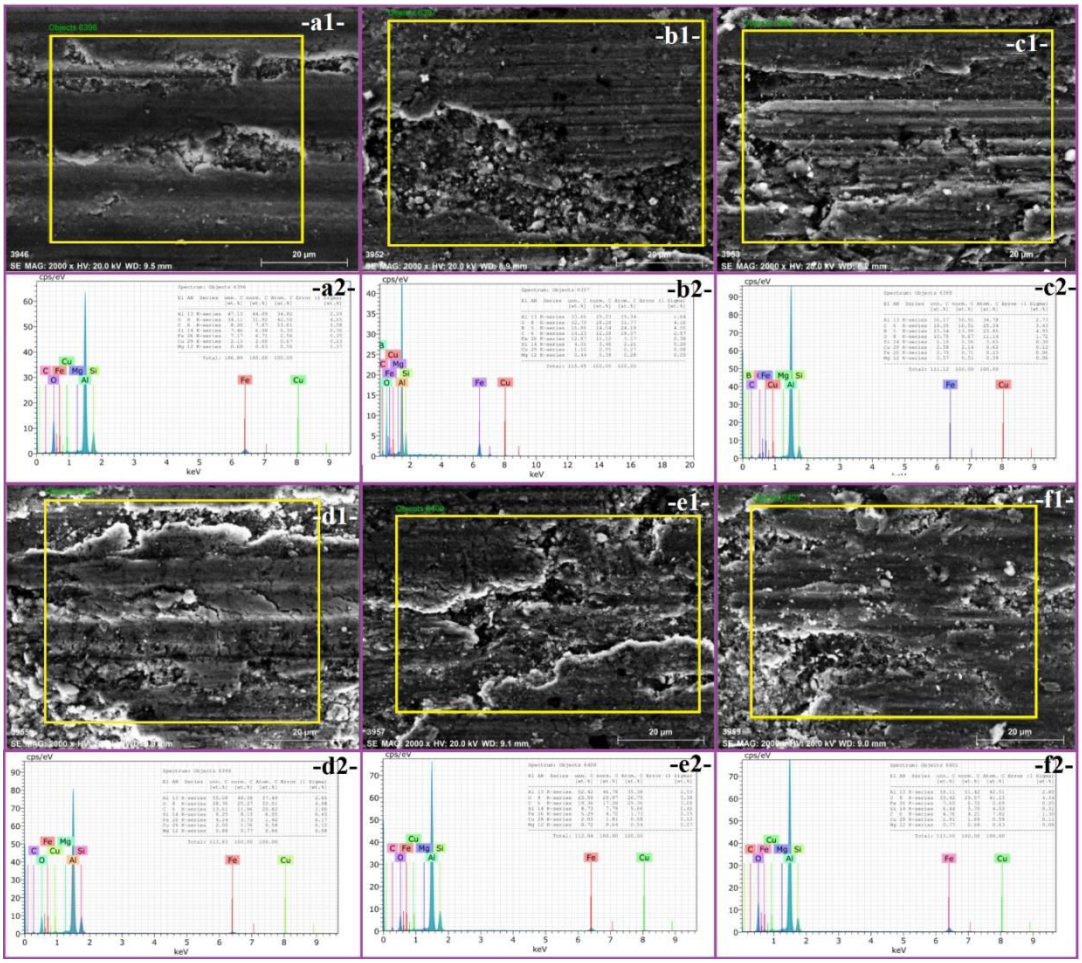

Fig. 9. Worn surface FESEM images of samples and element distribution rates (a) CS-550/60, (b) 10-CS-550/60, (c) MWS-550/0, (d) 10-MWS-550/0, (e) SPS-450/5, (f) 10-SPS-450/5.

4. Conclusion

The results of this experimental study are summarized below.

- In CS and MWS samples, B_4C particles are clustered at matrix grain boundaries and/or intergranular pores. In addition, interfacial bonding was partially formed between the matrix grains and between the matrix grains/B_4C particles. In SPS samples, a less porous and continuous interface was formed between the matrix grains and matrix grains/B_4C particles.
- While samples produced with CS and MWS techniques gave similar density values, samples produced with SPS gave the highest density values. A decrease in density was determined with the addition of B_4C particles in samples produced with different sintering techniques. However, this decrease in densities was limited to ≈2%.
- Compact samples produced with CS and MWS gave hardness values close to each other. When CS and MWS samples are compared, the difference in hardness between them is ≈5%. SPS samples gave the highest hardness values. An approximately 40% increase in the hardness values of SPS samples was determined compared to CS and MWS samples. The addition of 10 wt% B_4C caused a decrease in hardness. While this decrease in

hardness is approximately 11% in CS and MWS samples, it is approximately 5% in SPS samples.

- For 10 wt% B_4C reinforced and unreinforced samples, the highest volume loss and, thus, the lowest wear resistance were determined in the samples produced with CS. The lowest volume loss, that is, the highest wear resistance, was obtained in the samples produced with SPS. In general, the addition of B_4C negatively affected the wear performance in all samples. B_4C reinforced, and unreinforced SPS samples exhibited the lowest average CoF values. While CS and MWS samples gave higher CoF values than SPS samples, no significant change was found in terms of CoF values when CS and MWS samples were compared.
- Depending on the sintering techniques, different worn surface images were formed on the samples after wear. Different wear errors, such as wear debris, adhesion, smearing, delimination and ruptures were determined after wear. In addition to the elements in the chemical composition of Alumix 231®, Fe and O elements were determined on worn surfaces.
- P/M samples produced with the SPS technique exhibited better microstructures than MWS and CS samples. Therefore, SPS samples provided very good data in terms of density, hardness, and wear performance. MWS and CS samples gave close values in terms of density and hardness values. However, MWS samples exhibited higher wear performance. Therefore, the fact that the sintering temperature and holding time parameters in the SPS technique are much lower than in the MWS and CS techniques offers significant advantages in terms of energy and time savings. The MWS technique is also superior to the CS technique when the same parameters are taken into account.

ORCID numbers:

Melika Ozer, https://orcid.org/0000-0003-1807-3585
Yavuz Kaplan, https://orcid.org/0000-0002-3144-9332
Alpay Ozer, https://orcid.org/0000-0001-8496-0305
Sinan Aksoz, https://orcid.org/0000-0003-4324-5043

5. References

1. Khanna, V. Kumar, S.A. Bansal, Mechanical properties of aluminium-graphene/carbon nanotubes (CNTs) metal matrix composites: Advancement, opportunities and perspective. Mater. Res. Bull. 138 (2021) 111224.
2. Puchy, M. Podobova, R. Dzunda, P. Hvizdos, O. Velgosova, M. Besterci, B. Ballokova, Graphene nanoplatelets reinforced aluminum alloy matrix composites produced by spark plasma sintering, Kovove Mater. 59 (2021) 237–244.
3. W.G.E. Mosher, G.J. Kipouros, W.F. Caley, I.W. Donaldson, D.P. Bishop, On hot deformation of aluminium–silicon powder metallurgy alloys, Powder Met. 54 (2011) 366–375.
4. J. Zeng, C. Zhu, W. Wang, X. Li, H. Li, Evolution of primary Si phase, surface roughness and mechanical properties of hypereutectic Al–Si alloys with different Si contents and cooling rates, Phil. Mag. Lett. 100 (2020) 581–587.
5. D. Kumar, R.K. Phanden, L. Thakur, A review on environment friendly and lightweight magnesium-based metal matrix composites and alloys, Mater. Today-Proc. 38 (2021) 359–364.

6. I.A. Ibrahim, F.A. Mohamed, E.J. Lavernia, Particulate reinforced metal matrix composites-a review, J. Mater. Sci. 26 (1991) 1137–1156.
7. Ensar Kareem, Cabir Ebu Kudeiri, Asarudheen Abdudeen,Thanveer Ahammed, and Aiman Ziout, A Review on AA 6061 Metal Matrix Composites Produced by Stir Casting, Materials, 14(1) (2021) 175.
8. Naseem Ahamad, Aas Mohammad, Moti Lal Rinawa, Kishor Kumar Sadasivuni, Pallav Gupta, Correlation of structural and mechanical properties for Al-Al2O3-SiC hybrid metal matrix composites, Journal of Composite Materials, 2021, Vol. 55(23) 3267–3280.
9. M Ozer, S I Aydogan, H Cinici, A Ozer. Effects of sintering techniques and parameters on microstructure and mechanical properties of Al-15Si-2,5Cu-0.5Mg compacts and Al-15Si-2,5Cu-0.5Mg/B_4C composites. Materials Today Communications, 30 (2022) 103192.
10. Nan Kang, Mohammed EL Mansori, A new insight on induced-tribological behaviour of hypereutectic Al-Si alloys manufactured by selective laser melting, Tribology International, 149 (2020) 105751.
11. Esmaeil Damavandi, Salman Nourouzi, Sayed Mahmood Rabiee, Roohollah Jamaati, Ahmed A.Tiamiyu, Jerzy A.Szpunar, Effects of prior ECAP process on the dynamic impact behaviors of hypereutectic Al-Si alloy, Materials Science and Engineering: A, 793, 19 (2020) 139902.
12. Masoumeh Faraji, A New Approach in Numerical Modeling of Inoculation of Primary Silicon in a Hypereutectic Al-Si Alloy, Metallurgical and Materials Transactions B, 52 (2021) 778–791.
13. T. . Saravanana, M. Kamaraj, S. C. Sharma, S. Anoop, Sushant K. Manwatkar, K. V.Ravikanth, A. Venugopal, S. Kumaran, Influence of characteristic eutectic free microstructure on mechanical and corrosion response of spark plasma sintered hypereutectic Al-Si alloy, Materials Letters, Volume 308, Part A, 1 (2022) 131104.
14. S.C. Tjong, Z.Y. Ma, Microstructural and mechanical characteristics of in situ metal matrix composites, Materials Science and Engineering: R: Reports, Volume 29, Issues 3–4, 15 (2000) 49–113.
15. J.W.Kaczmar, K.Pietrzak, W.Włosiński, The production and application of metal matrix composite materials, Journal of Materials Processing Technology, 106, 1-3 (2000) 58–67.
16. Y Kaplan, S Aksöz, H Ada, E. İnce, S Özsoy, The effect of aging processes on tribo-metallurgy properties of al based ternary alloys product by P/M technique, Sci. Sinter. 52 (2020) 445–456.
17. G. Altuntaş, A. T.Özdemir, & B. Bostan, A survey of the effect of cryogenic treatment and natural ageing on structural changes and second-phase precipitation in Al–Zn–Mg–Cu alloy. Journal of Thermal Analysis and Calorimetry, 148(20) (2023) 10713–10725.
18. A. Ozer, The microstructures and mechanical properties of Al-15Si-2.5Cu-0.5Mg/(wt%)B_4C composites produced through hot pressing technique and subjected to hot extrusion, Mater. Chem. Phys. 183 (2016) 288–296.
19. D.W. Heard, I.W. Donaldson, D.P. Bishop. Metallurgical assessment of a hypereutectic aluminum–silicon P/M alloy. J. Mater Process Tech., 209 (2009) 5902–5911.
20. I. Arribas, J.M. Martin, F. Castro. The initial stage of liquid phase sintering for an Al–14Si–2.5Cu–0.5Mg (wt%) P/M alloy. Mat. Sci. Eng. A Struct., 527 (2010) 3949–3966.
21. Rudinsky, J.M. Aguirre, G. Sweet, J. Milligan, D.P. Bishop, M. Brochu. Spark plasma sintering of an Al-based powder blend. Mat. Sci. Eng. A Struct., 621 (2015) 18–27.

22. A. Manonukul, A. Salee. Relationship between atmospheric dew point and sinterability of Al-Si based alloy. J. Mater Sci. Technol., 29 (1) (2013) 70–76.
23. Saheb N., Iqbal, Z., Khalil, A., Hakeem, A. S., Aqeeli, N-A., Laoui, T., Al-Qutub, A., and Kirchner, R. Spark plasma sintering of metals and metal matrix nanocomposites: A review. Journal of Nanomaterials, (2012) 1–13.
24. M Ozer, S I Aydogan, A Ozer, H Cinici, E Ayas, Influence of spark plasma sintering and conventional sintering on microstructure and mechanical properties of hypereutectic Al-Si alloy and hypereutectic Al-Si/B_4C composites, Kovove Materialy, 60, 6 (2022) 387–396.
25. Z Shen, M Johnsson, Z Zhao, M Nygren, Spark Plasma Sintering of Alumina. J. Am. Ceram. Soc., 85 (2002) 1921–1927.
26. J.E. Zorzi, C.A. Perottoni, J.A.H. da Jornada, Hardness and wear resistance of B_4C ceramics prepared with several additives, Materials Letters, 59, 23 (2005) 2932–2935.
27. Park, J.W., Lee, H.C. & Lee, S. Composition, microstructure, hardness, and wear properties of high-speed steel rolls. Metall Mater Trans A, 30 (1999) 399–409.
28. Jin-Kun Xiao, Hong Tan, Juan Chen, Ashlie Martini, Chao Zhang, Effect of carbon content on microstructure, hardness and wear resistance of CoCrFeMnNiCx high-entropy alloys, Journal of Alloys and Compounds, 847 (2020) 156533.
29. T. Sathish, S. Saravanan, V. Vijayan, Effect of reinforced aluminium alloy LM30 with pure ceramic particles to evaluate hardness and wear properties, Materials Research Innovations, 24 (3) (2020) 129–132.
30. Z. Zak Fang, Xu Wang, Taegong Ryu, Kyu Sup Hwang, H.Y. Sohn, Synthesis, sintering, and mechanical properties of nanocrystalline cemented tungsten carbide – A review, International Journal of Refractory Metals and Hard Materials, Volume 27, Issue 2, March 2009, Pages 288-299. https://doi.org/10.1016/j.ijrmhm.2008.07.011
31. N. Showaiter, M. Youseffi, Compaction, sintering and mechanical properties of elemental 6061 Al powder with and without sintering aids, Materials & Design, 29, 4 (2008) 752–762.
32. R. M. Anklekar, D. K. Agrawal, R. Roy, Microwave sintering and mechanical properties of PM copper steel, Powder Metallurgy, 44(4) (2001) 355–362.
33. Z.D. I Sktani, A Arab, J J Mohamed, Z A Ahmad, Effects of additives additions and sintering techniques on the microstructure and mechanical properties of Zirconia Toughened Alumina (ZTA): A review, International Journal of Refractory Metals and Hard Materials, 106 (2022) 105870.
34. Aksöz, S., Bostan, B. Effects of the AA2014/B4C MMCs production with casting and post casting sintering operations on wear behaviors. Journal of Boron, 3(2) (2018) 132–137.
35. Aksöz Sinan, "The effect of aging temperature and aging duration on the dry sliding wear behavior of Ti6Al4V alloy", Science of Sintering, 55 (4) (2023) 527–538.
36. Aksöz S, Kaner S, Kaplan Y, Tribological and aging behavior of hybrid Al 7075 composite reinforced with B4C, SiC, and TiB2, Sci. Sinter. 53 (2021) 311-321.
37. Ozyurek D, Ciftci I, An investigation into the wear behaviour of TiB2 particle reinforced aluminium composites produced by mechanical alloying, Sci. Eng. Compos. Mater. 18 (1-2) (2011) 5–12.
38. Saka N, Eleiche AM, Suh NP, Wear of metals at high sliding speeds, Wear, 44 (1) (1977) 109–125.

Сажетак: *У овој студији испитивани су утицаји различитих техника синтеровања и додавања B_4C честица на микроструктурна својства, густину, тврдоћу и абразивно хабање. Експерименти хабања су изведени у складу са ASTM стандардом G99 коришћењем пин-он-диск апарата у условима сувог испитивања. Испресовани узорци*

произведени конвенционалним и микроталасним синтеровањем дали су вредности густине и тврдоће блиске једна другој. У узорцима произведеним техником синтеровања у плазми, стопа порозности је најнижа, а тврдоћа највећа. У узорцима произведеним различитим техникама синтеровања, додавање B_4C честица изазвало је повећање порозности и смањење густине и тврдоће. Најнижа отпорност на хабање код свих узорака утврђена је код узорака произведених конвенционалним синтеровањем. Најмањи губитак запремине, односно највећа отпорност на хабање, добијен је у узорцима произведеним синтеровањем у плазми. Генерално, додавање B_4C негативно је утицало на перформансе хабања у свим узорцима.

***Кључне речи**: Синтеровање, хабање, композит, Al легура.*